

The SOPHIE search for northern extrasolar planets [★]

VI. Three new hot Jupiters in multi-planet extrasolar systems

Moutou, C.¹, Hébrard, G.^{2,3}, Bouchy, F.^{1,4}, Arnold, L.³, Santos, N.C.^{5,10}, Astudillo-Defru, N.⁶, Boisse, I.⁵, Bonfils, X.⁶, Borgniet, S.⁶, Delfosse, X.⁶, Díaz, R. F.¹, Ehrenreich, D.⁴, Forveille, T.⁶, Gregorio, J.⁷, Labrevoir, O.⁸, Lagrange, A.-M.⁶, Montagnier, G.^{3,2}, Montalto, M.⁵, Pepe, F.⁴, Sahlmann, J.⁴, Santerne, A.⁵, Ségransan, D.⁴, Udry, S.⁴, and Vanhuyse, M.⁹

¹ Aix Marseille University, CNRS, LAM (Laboratoire d'Astrophysique de Marseille) UMR 7326, 13388 Marseille cedex 13, France
e-mail: Claire.Moutou@oamp.fr

² Institut d'Astrophysique de Paris, UMR 7095 CNRS, Université Pierre & Marie Curie, 98bis boulevard Arago, 75014 Paris, France

³ Observatoire de Haute-Provence, CNRS & OAMP, 04870 Saint-Michel l'Observatoire, France

⁴ Observatoire de Genève, Université de Genève, 51 Chemin des Maillettes, 1290 Sauverny, Switzerland

⁵ Centro de Astrofísica, Universidade do Porto, Rua das Estrelas, 4150-762 Porto, Portugal

⁶ UJF-Grenoble 1 / CNRS-INSU, Institut de Planétologie et d'Astrophysique de Grenoble (IPAG) UMR 5274, Grenoble, F-38041, France

⁷ Atalaia group, Crow Observatory-Portalegre, Portugal

⁸ Centre d'Astronomie, Plateau du Moulin à Vent, 04870 Saint-Michel-l'Observatoire, France

⁹ Oversky, 47 Allée des Palanques, 33127 Saint Jean d'Ilac, France

¹⁰ Departamento de Física e Astronomia, Faculdade de Ciências, Universidade do Porto, Portugal

Preprint online version: October 16, 2018

ABSTRACT

We present high-precision radial-velocity measurements of three solar-type stars: HD 13908, HD 159243, and HIP 91258. The observations were made with the SOPHIE spectrograph at the 1.93-m telescope of Observatoire de Haute-Provence (France). They show that these three bright stars host exoplanetary systems composed of at least two companions. HD 13908 b is a planet with a minimum mass of $0.865 \pm 0.035 M_{\text{Jup}}$ on a circular orbit with a period of 19.382 ± 0.006 days. There is an outer massive companion in the system with a period of 931 ± 17 days, $e = 0.12 \pm 0.02$, and a minimum mass of $5.13 \pm 0.25 M_{\text{Jup}}$. The star HD 159243 also has two detected companions with respective masses, periods, and eccentricities of $M_p = 1.13 \pm 0.05$ and $1.9 \pm 0.13 M_{\text{Jup}}$, $P = 12.620 \pm 0.004$ and 248.4 ± 4.9 days, and $e = 0.02 \pm 0.02$ and 0.075 ± 0.05 . Finally, the star HIP 91258 has a planetary companion with a minimum mass of $1.068 \pm 0.038 M_{\text{Jup}}$, an orbital period of 5.0505 ± 0.0015 days, and a quadratic trend indicating an outer planetary or stellar companion that is as yet uncharacterized. The planet-hosting stars HD 13908, HD 159243, and HIP 91258 are main-sequence stars of spectral types F8V, G0V, and G5V, respectively, with moderate activity levels. HIP 91258 is slightly over-metallic, while the two other stars have solar-like metallicity. The three systems are discussed in the frame of formation and dynamical evolution models of systems composed of several giant planets.

Key words. Planetary systems – Techniques: radial velocities – Techniques: photometry – Stars: individual: HD 13908, HD 159243, HIP 91258

1. Introduction

Radial-velocity surveys have continuously provided new extra-solar planetary candidates since 1995 (Mayor & Queloz 1995). The observing strategy, consisting of multiple observations of single stars, is time-consuming and requires long-term programs on quasi-dedicated telescopes. These observations are necessary, however, to achieve a complete picture of the exoplanet population, especially towards the most populated long-period or/and low-mass ends. Statistical analyses were recently published by Mayor et al. (2011), Howard et al. (2010), and Wright et al. (2012), indicating the frequency of stars that harbour close-in

massive planets - also called hot Jupiters: Mayor et al. (2011) reported a value of $0.89 \pm 0.36\%$ for the occurrence of planets more massive than $50M_{\oplus}$ that have periods shorter than 11 days, Howard et al. (2010) found an occurrence of $1.2 \pm 0.2\%$ for planets more massive than $100M_{\oplus}$ with periods shorter than 12 days and Wright et al. (2012) estimated $1.2 \pm 0.38\%$ for planets more massive than $30M_{\oplus}$ with periods shorter than 10 days. In the Kepler survey, which has a different target sample, 0.43% of stars are found to harbour giant planets with radii between 6 and 22 Earth radii and periods shorter than 10 days (Howard et al. 2012; Fressin et al. 2013). The frequency of planets then increases towards lower masses, to reach more than 50% of the stars (Mayor et al. 2011) within the current detection limits of the available instruments. Hot Jupiters are thus extremely rare objects, although they have been at the heart of exoplanetary science for more than fifteen years, particularly for detailed characterizations, such as atmospheric studies and observations.

Send offprint requests to: Claire.Moutou@lam.fr

[★] Based on observations collected with the SOPHIE spectrograph on the 1.93-m telescope at Observatoire de Haute-Provence (CNRS), France, by the SOPHIE RPE Consortium (program PNP.CONNS). Table 8 is only available in electronic form at the CDS via anonymous ftp to cdsarc.u-strasbg.fr (130.79.128.5).

In this paper, we report the discovery of three new planets with orbital periods shorter than 20 days and projected masses of about one Jupiter mass. Interestingly, they are the inner planets in a multiple system, with a more massive second companion in the external part of the system. These discoveries were made in the context of a large program with SOPHIE, the high-precision radial-velocity spectrograph at the Observatoire de Haute-Provence. The survey for giant planets occupies about 12% of the telescope time since 2006 and has already allowed the discovery of twelve companions in the planet or brown dwarf range (da Silva et al. 2007; Santos et al. 2008; Bouchy et al. 2009; Hébrard et al. 2010; Boisse et al. 2010; Díaz et al. 2012). In Section 2, we describe the observations and analyses, in Section 3 we report the stellar properties, and in Section 4 we show and analyse the radial-velocity observations. In Section 5, we discuss the results and conclude.

2. Spectroscopic observations

The spectroscopic observations were obtained with the SOPHIE spectrograph at the Observatoire de Haute-Provence with the 1.93-m telescope in the framework of the large program (PNP.CONNS) led by the SOPHIE Exoplanet Consortium, presented in detail by Bouchy et al. (2009). The SOPHIE instrument (Perruchot et al. 2011) is a fiber-fed environmentally stabilized echelle spectrograph covering the visible range from 387 to 694 nm. The spectral resolving power is 75,000 in high-resolution mode.

The radial velocities (RV) are obtained by cross-correlating the extracted spectra with a numerical mask based on stellar spectra, following the method developed by Baranne et al. (1996) and Pepe et al. (2002). For all three stars the numerical mask corresponding to a G2 spectral type was used because it provides the smallest individual error bars and residual scatter compared with the other available F0 and K5 masks.

The spectrograph has been upgraded in two steps (Bouchy et al. 2013), resulting in a slight zero-point motion at dates JD-2,400,000 = 55,730 and 56,274. The first update corresponds to the installation of a section of octagonal fibers upstream of the double scrambler, the second one to another section of octagonal fibers downstream; SOPHIE+ labels the measurements obtained after the updates. When applicable, the data sets should thus be taken as independent, with a free offset to be adjusted together with the Keplerian solution. The velocity offset between SOPHIE and SOPHIE+ is $11 \pm 10 \text{ m s}^{-1}$ for HD 13908 and $37 \pm 12 \text{ m s}^{-1}$ for HD 159243. They agree at 1.2σ , converging into a $24 \pm 12 \text{ m s}^{-1}$ velocity shift for solar-like stars. The error on this offset propagates into the parameters of the orbits, with the largest impact on the errors on the mass and period of the outer planets.

In the context of the program where HD 13908, HD 159243, and HIP 91258 were observed, the objective was to obtain multiple measurements on a large sample of stars at a moderate RV precision. A signal-to-noise ratio of 50 only is aimed at, which gives an average noise level of 5 m s^{-1} for individual measurements.

The radial-velocity measurements of the three stars are given in Tables 5, 6 and 7.

3. Stellar properties

The SOPHIE spectra were used to spectroscopically determine stellar parameters. The method described in Santos et al. (2004)

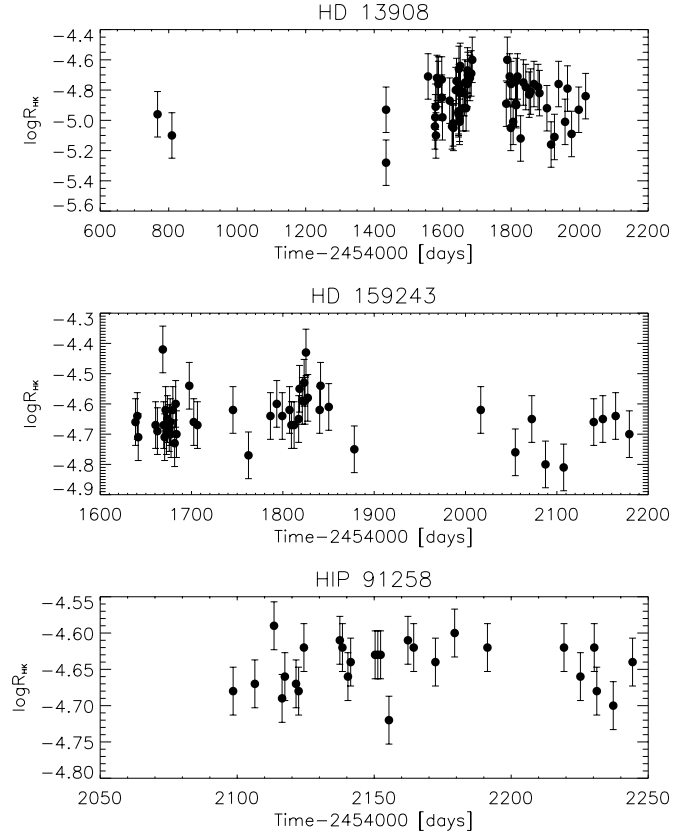


Fig. 1. Variations with time of the $\log R'_{\text{HK}}$ activity index for HD 13908 (top), HD 159243 (middle), and HIP 91258 (bottom).

Table 1. Observed and inferred stellar parameters for the planet-hosting stars. Uncertainties are noted between brackets. The horizontal line separates the parameters given in van Leeuwen (2007) and the parameters derived in this paper.

Parameter	HD 13908	HD 159243	HIP 91258
Sp	F8V	G0V	G5V
V	7.51 (0.01)	8.65 (0.01)	8.65 (0.01)
$B - V$ [mag]	0.53	0.54	0.80
π [mas]	14.05 (0.70)	14.45 (1.14)	22.26 (0.66)
d [pc]	71.2 (3.5)	69.2 (5.5)	44.9 (1.3)
M_V [mag]	3.25	4.45	5.39
$B.C.$ [mag]	-0.016	-0.030	-0.134
L [L_{\odot}]	4.0	1.3	0.6
T_{eff} [K]	6255 (66)	6123 (65)	5519 (70)
$\log g$ [cgs]	4.11 (0.11)	4.55 (0.11)	4.53 (0.12)
[Fe/H] [dex]	0.01 (0.04)	0.05 (0.04)	0.23 (0.05)
M_* [M_{\odot}]	1.29 (0.04)	1.125 (0.03)	0.95 (0.03)
$v \sin i$ [km s^{-1}]	4.2 (0.5)	3.8 (0.5)	3.5 (0.5)
$\log R'_{\text{HK}}$	-4.9 (0.2)	-4.65 (0.1)	-4.65 (0.1)
Age [Gy]	2.9 (0.4)	1.25 (1.1)	2.4 (2.4)
R_* [R_{\odot}]	1.67 (0.1)	1.12 (0.05)	1.0 (0.04)

and Sousa et al. (2008) was used on the mean high-signal-to-noise-ratio spectrum obtained for each star. We derived the effective temperature T_{eff} , gravity $\log g$, and the iron content of the stellar atmospheres of HD 13908, HD 159243, and HIP 91258 using equivalent width measurements of the Fe I and Fe II weak lines by imposing excitation and ionization equilibrium assuming local thermal equilibrium. Errors were obtained by quadrat-

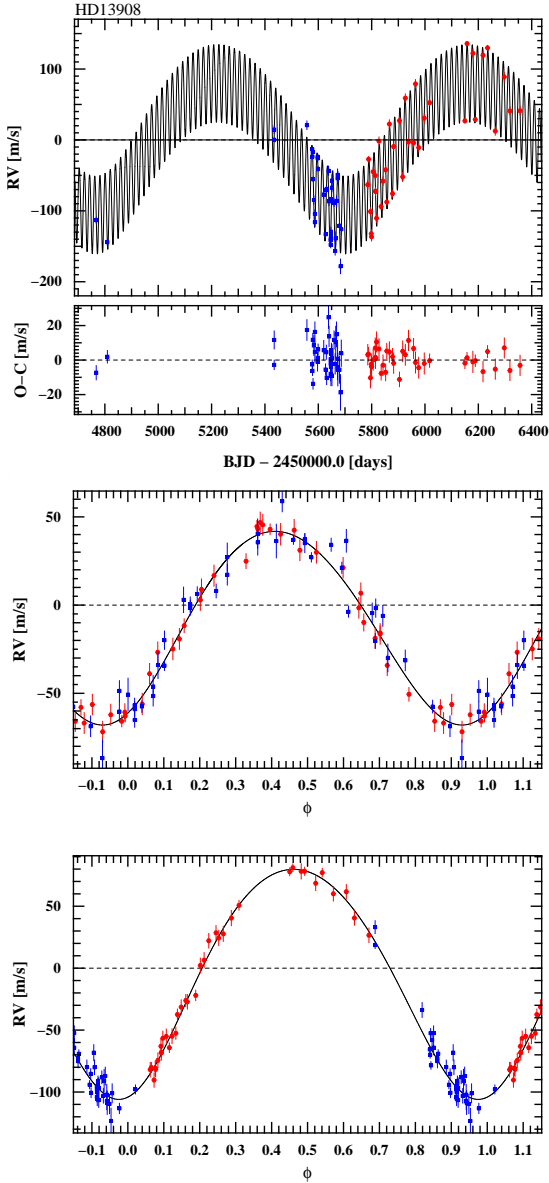


Fig. 2. SOPHIE radial velocities and Keplerian model of the HD 13908 system: (top) as a function of time, with the residuals; (middle) as a function of phase for the inner planet; (bottom) as a function of phase for the outer planet. The blue points correspond to SOPHIE data obtained before June 2011, the red points corresponds to more recent measurements after the SOPHIE+ upgrade.

ically adding respectively 60 K, 0.1, and 0.04 dex to the internal errors on T_{eff} , $\log g$, and $[\text{Fe}/\text{H}]$.

The new reduction of the Hipparcos data (van Leeuwen 2007) was used to obtain the stellar parallaxes and derive the stellar luminosities after including the bolometric corrections proposed by Flower (1996) for the given effective temperatures. Then, the stellar mass, radius, and ages were derived using the evolutionary tracks and Bayesian estimation of da Silva et al. (2006). To take into account systematic effects, we adopted conservative uncertainties of 10% on the stellar mass.

The results are summarized in Table 1. All three stars are solar-like dwarfs. HD 13908 and HD 159243 have solar metallicity, while HIP 91258 has a significant excess of metal compared with the Sun, with $[\text{Fe}/\text{H}] = 0.23 \pm 0.05$.

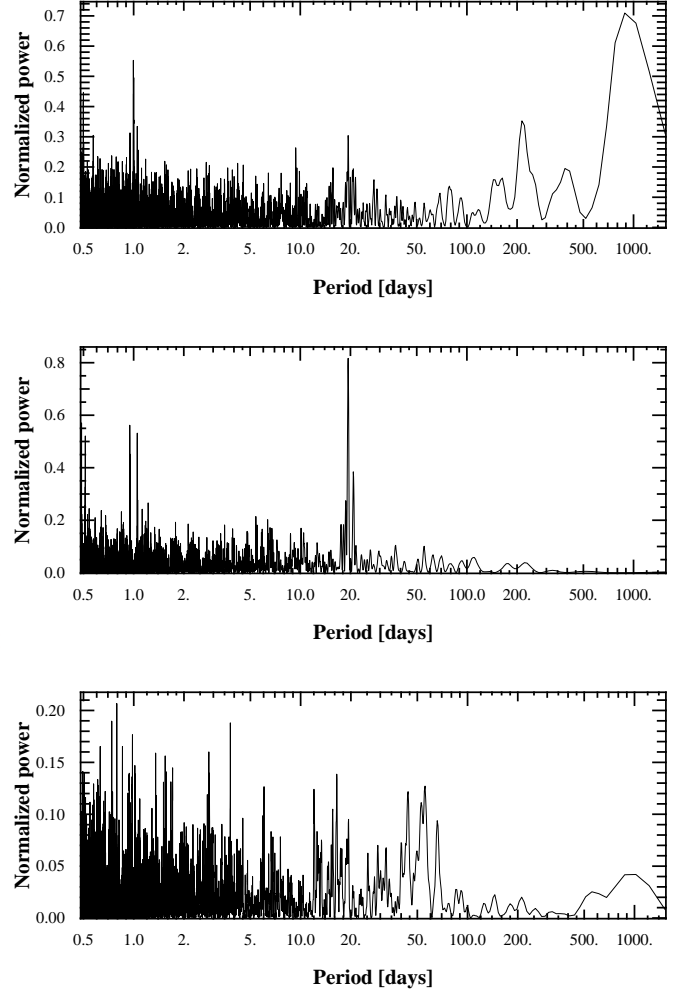


Fig. 3. Periodogram of the radial velocity measurements of HD 13908 with both signals (top), with the outer-planet signal removed (middle), and periodogram of the bisector span (bottom).

The cross-correlation function allows various stellar indicators to be estimated: the bisector span (tracer of activity and blended stellar systems) and the projected rotational velocity (using calibrations developed in Boisse et al. (2010)). In addition, the activity level of the stellar chromosphere was estimated from the calcium H and K equivalent widths. The average value of the $\log R'_{\text{HK}}$ parameter is also given in Table 1. While HD 13908 is not active ($\log R'_{\text{HK}} = -4.9$ dex), HD 159243 and HIP 91258 have a relatively high activity level ($\log R'_{\text{HK}} = -4.65$ dex for both). The variations of the $\log R'_{\text{HK}}$ value with time were systematically checked (Figure 1) to verify whether the slow radial-velocity modulation is due to the long-term cycles of the star (Dumusque et al. 2011). Then, the bisector variations were inspected to determine whether they correlate with the radial-velocity signal at each detected period. A negative correlation between the bisector spans and the radial velocities usually indicates that the distortion of stellar lines due to spot activity produces radial-velocity jitter (Queloz et al. 2001; Boisse et al. 2012), and the planet interpretation may be compromised. The expected jitter due to activity is of the order of 9, 12, and 12 m s^{-1} for HD 13908, HD 159243, and HIP 91258, respectively, using calibrations described in Santos et al. (2000).

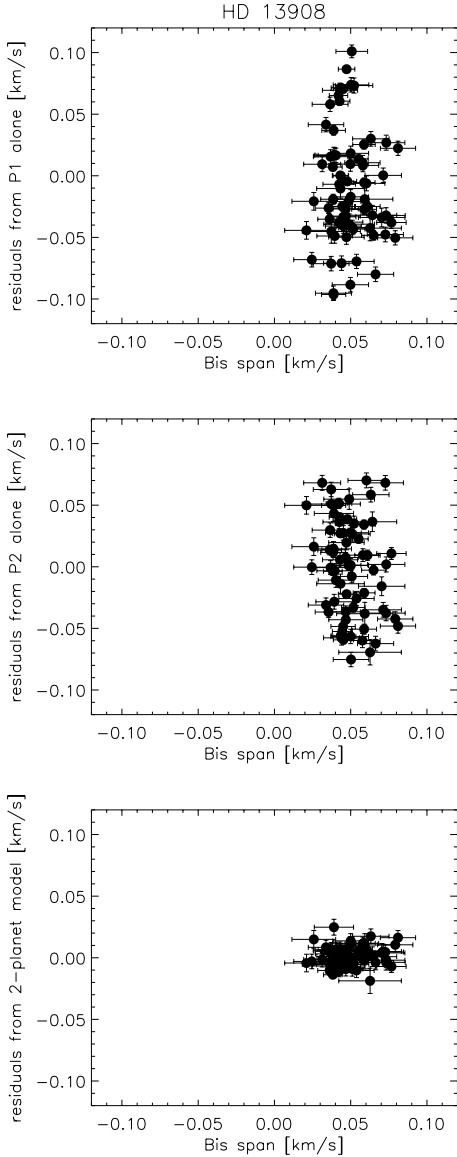


Fig. 4. Bisector variations as a function of radial-velocity residuals from HD 13908 SOPHIE measurements, (top) without the outer planet signal, (middle) without the inner planet signal, and (bottom) without both planet signals.

Finally, ranges for the rotation periods can be estimated from the $B - V$ and $\log R'_{\text{HK}}$ values. We found ranges of 5-9, 3-16, and 17-30 days, using the equations in Noyes et al. (1984) and a 3σ error range on $\log R'_{\text{HK}}$.

4. Radial-velocity analysis

4.1. HD 13908

Seventy-seven SOPHIE measurements have been collected on the star HD 13908 during more than four years between October 2008 and January 2013. The average noise of individual measurements is 7.9 m s^{-1} using SOPHIE, and 5.2 m s^{-1} using SOPHIE+ (Fig. 2). The radial-velocity fluctuations have a stan-

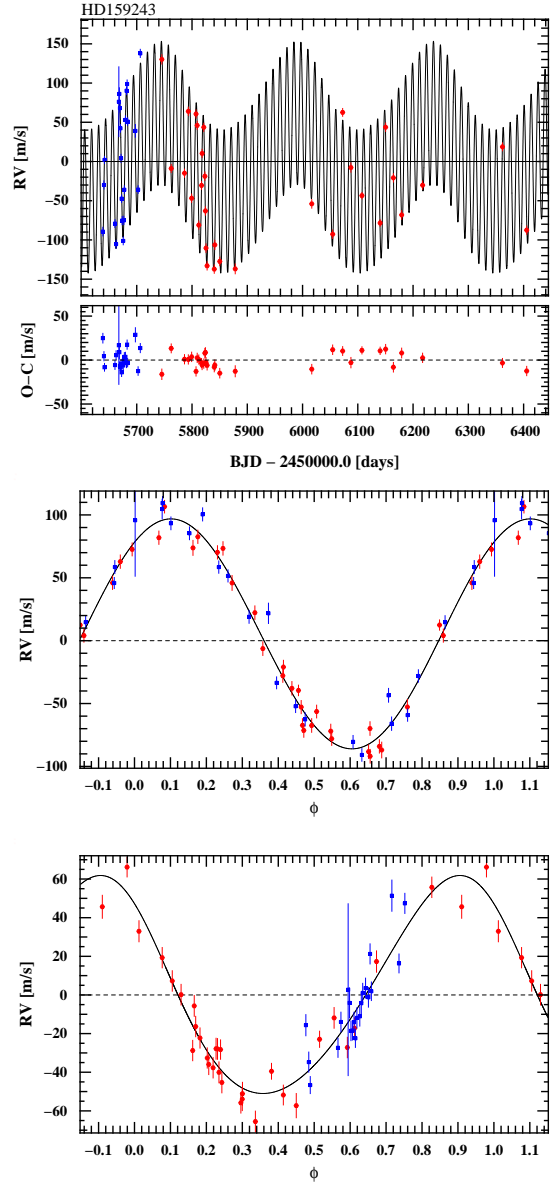


Fig. 5. SOPHIE radial velocities and Keplerian model of the HD 159243 system. The display is the same as in Fig. 2, i.e. the middle and bottom panel correspond to the inner and outer planet, respectively.

dard deviation of 74 m s^{-1} , with a short-term component and a longer-term component. Because the measurements were secured in both the SOPHIE and SOPHIE+ configurations (Table 5), we split the data set into two parts (delimited by the horizontal line in the table).

Several solutions were tried and compared by estimating the standard deviation of the residuals: single-planet model, single-planet model with linear and quadratic trend, two-planet model, two-planet model with trends, and three-planet models. The best solution was found with a two-Keplerian model with respective semi-amplitudes of 55.3 ± 1.2 and $90.9 \pm 3.0 \text{ m s}^{-1}$ (Fig. 2). The periodograms of the RV measurements are shown in Fig. 3. The peak corresponding to the outer companion is shown in the top plot; when the long-period signal is removed from the data, the inner-planet peak becomes prominent (middle plot). The residuals of the two-planet model have an r.m.s. of 9.6 m s^{-1} for the first data set, and 5.3 m s^{-1} for the second data set after the

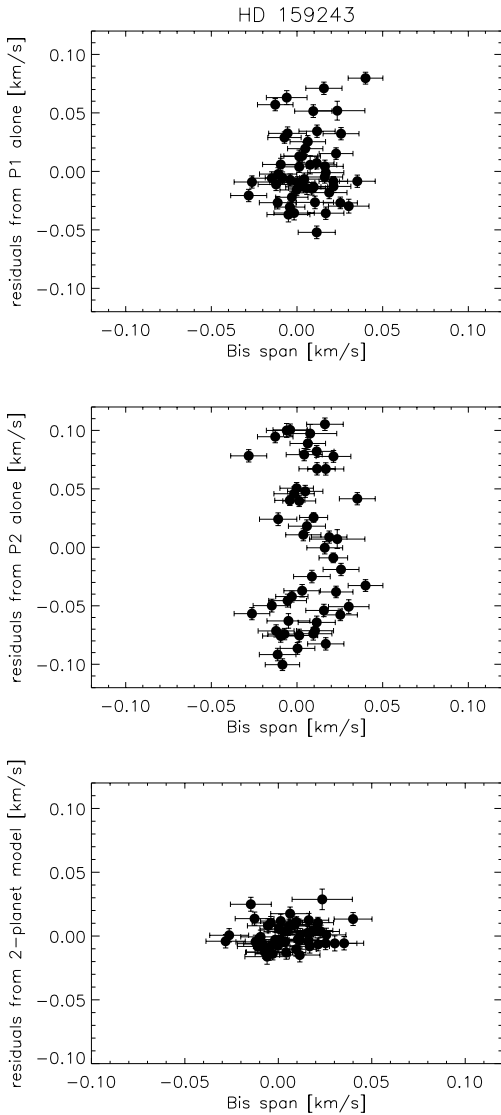


Fig. 6. Bisector variations as a function of radial-velocity residuals for HD 159243. Same plots as in Fig. 4.

spectrograph’s upgrade. These residual values are close to the one predicted from the activity jitter of 9 m s^{-1} in Santos et al. (2000) and may be attributed to the stellar photospheric activity.

We searched in vain for periodicity in the time series of the bisector span (Fig. 3 bottom) and the chromospheric index $\log R'_{\text{HK}}$, therefore it seems unlikely that the short-period signal is generated by the rotation period of the star or that the long-period signal is related to the activity cycle of HD 13908 (Dumusque et al. 2011). The bisector spans do not vary with the radial velocity for any of the detected signals, which rules out that the photospheric activity is the main source of the variations (Figure 4). The origin of the two signals is most likely the Doppler shift of the stellar spectrum that is caused by the orbital motion of the planets around the star and not by the deformation of the stellar profile due to photospheric activity. Note that the

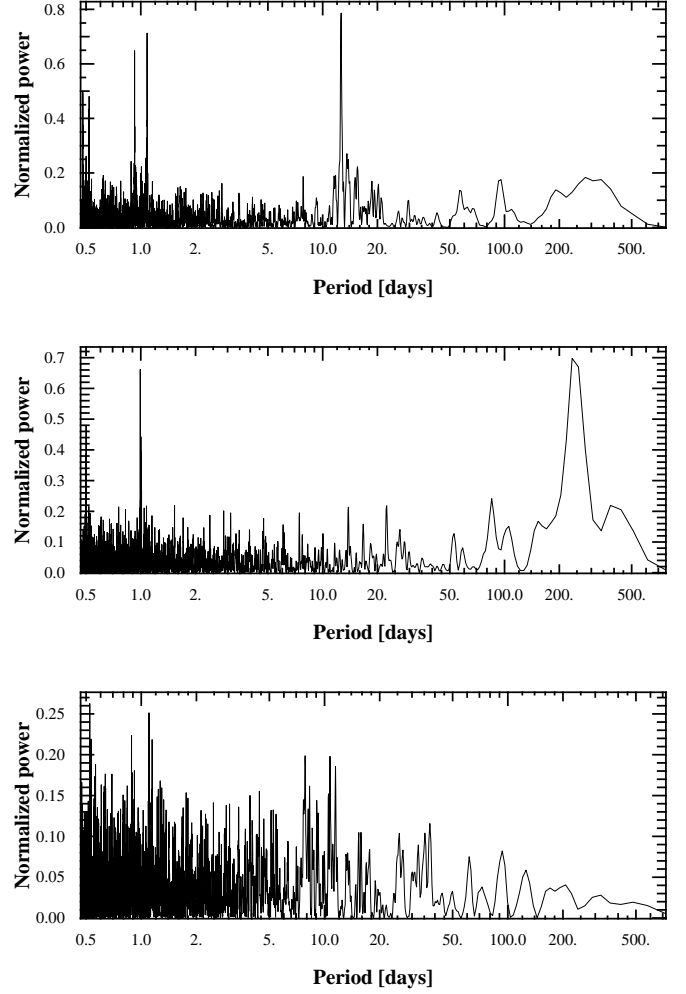


Fig. 7. Periodogram of the radial-velocity measurements of HD 159243 with both signals (top), without the inner-planet signal (middle), and the periodogram of the bisector span (bottom).

scatter of the bisector and $\log R'_{\text{HK}}$ activity indices are 13 m s^{-1} and 0.15 dex.

Because activity is discarded as a possible source of the radial-velocity variations, the system around HD 13908 is very likely composed of a Jupiter-like planet in a 19.4-day orbit and a massive giant planet in a 2.5-year long orbit. Parameters obtained with Monte Carlo Markov Chain simulations in *YORBIT*, using 500,000 iterations, are given in Table 2. Although the eccentricity of the inner planet is not significantly different from zero, we kept it as a free parameter to include the associated error in the general modeling of the system.

The short-period planet has a transit probability of 3%. Photometric observations were attempted. No transit was detected because we missed the transit window, as we realized later from the refined ephemeris. Additional observations are therefore encouraged at the transit times given by $JD = 2,455,756.032 + N \times 19.382$.

Finally, we searched the Hipparcos astrometry data for the signature of the outer companion with the method presented in Sahlmann et al. (2011). Since five orbital elements are determined by spectroscopy (P , e , T_0 , ω , K), the intermediate-astrometry data (van Leeuwen 2007) can constrain the two re-

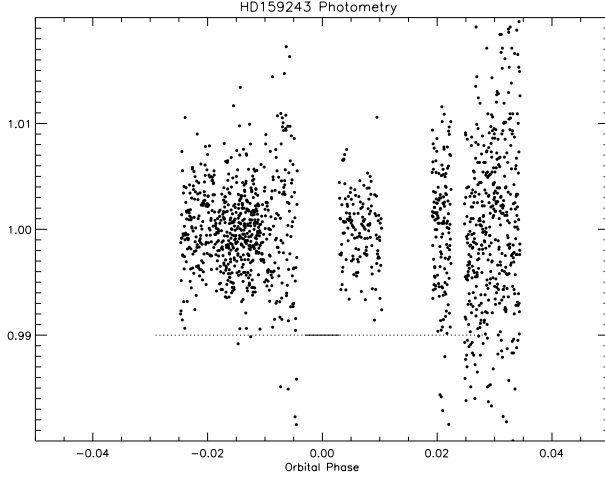


Fig. 8. Relative flux of HD 159243 phased with the orbital period and time of transit of companion b. The dotted line shows the $1\text{-}\sigma$ uncertainty in the transit ephemeris. The thick line shows the transit duration and expected transit depth for the nominal ephemeris. There is no evidence of a transit, although it cannot be ruled out in the whole range.

Table 2. Orbital and physical parameters for the planets orbiting the star HD 13908. T is the epoch of the highest RV. $\sigma(\text{O-C})$ is the residual noise after orbital fitting.

Parameter		HD 13908 b	HD 13908 c
P	[days]	19.382 ± 0.006	931 ± 17
T	[JD-2400000]	55750.93 ± 0.18	56165 ± 9
T_{transit}	[JD-2400000]	55756.032 ± 0.156	56436 ± 15
e		0.046 ± 0.022	0.12 ± 0.02
ω	[deg]	185 ± 43	185 ± 11
K	[m s^{-1}]	55.3 ± 1.2	90.9 ± 3.0
$m_2 \sin i$	[M_{Jup}]	0.865 ± 0.035	5.13 ± 0.25
a	[AU]	0.154 ± 0.0025	2.03 ± 0.04
γ_{SOPHIE}	[km s^{-1}]	15.893 ± 0.008	
$\gamma_{\text{SOPHIE+}}$	[km s^{-1}]	15.882 ± 0.006	
N_{meas}		77	
Span	[days]	1588.7	
$\sigma(\text{O-C})$	[m s^{-1}]	9.6/5.3	
χ_{red}^2		2.6	

maining orbital parameters, in particular the orbit inclination i that yields the companion's mass. No astrometric signature corresponding to the spectroscopic orbit was detected, which can be translated into a limit on i and an upper limit of $0.15 M_{\odot}$ for the mass of HD 13908 c. This constraint is compatible with the non-detection of a secondary signal in the cross-correlation function.

4.2. HD 159243

We secured fifty-three SOPHIE radial-velocity measurements of HD 159243 during 767 days, from March 2011 to April 2013. Thirty-two measurements were obtained after the SOPHIE+ upgrade. The total data set features individual error bars with an average of 5.2 m s^{-1} (Fig. 5). The standard deviation of the time series is 71 m s^{-1} . In the same way as for HD 13908, we compared several models with sets of 1, 2, or 3 planets and trends.

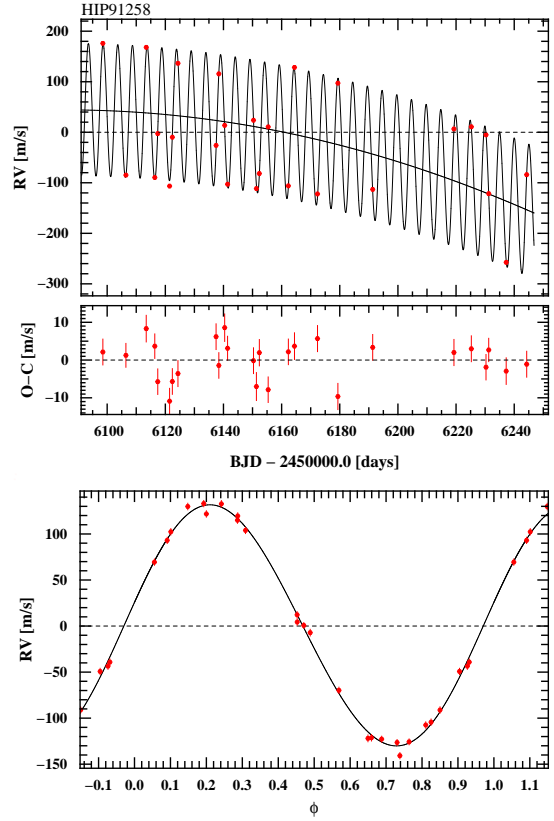


Fig. 9. SOPHIE radial velocities and Keplerian model of the system orbiting HIP 91258: (top) as a function of time, with the residuals to the model including a quadratic long-term trend, and (bottom) as a function of phase for the inner planet.

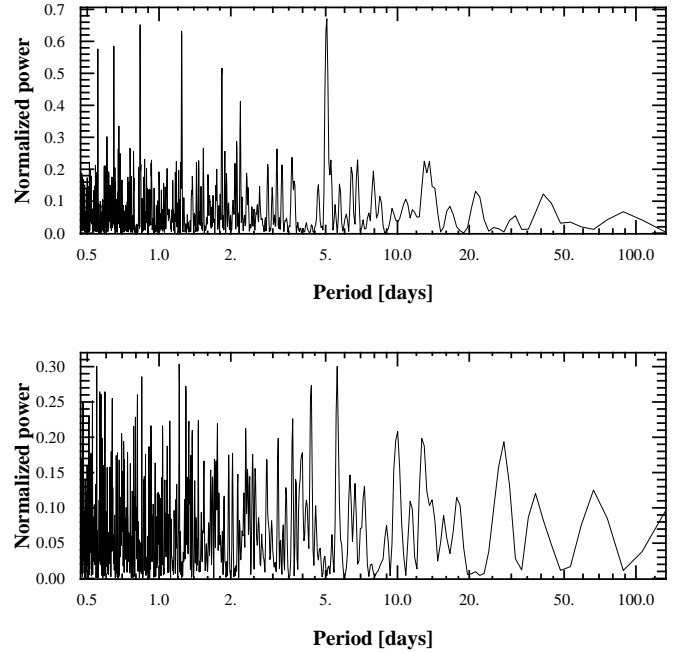


Fig. 10. Periodogram of the radial-velocity measurements of HIP 91258 (top) and of the bisector span (bottom).

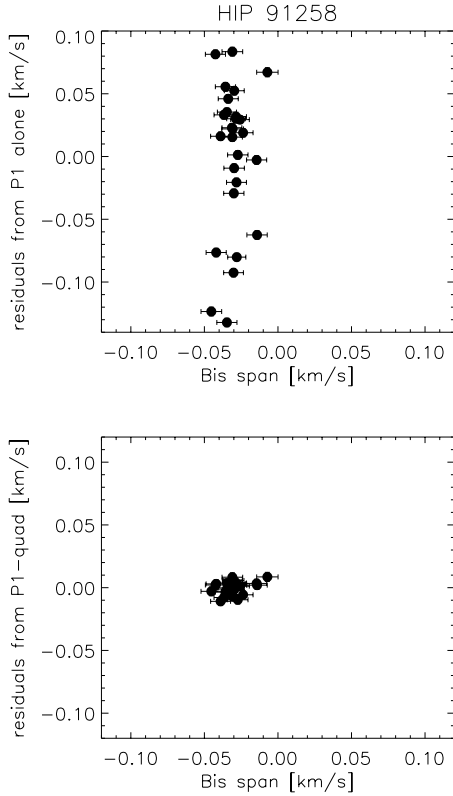


Fig. 11. Bisector variations as a function of radial-velocity residuals for HIP 91258. (top) without the 5.05-day period planet signal, and (bottom) without both the planet signal and the quadratic trend.

The best-fit model was obtained with two Keplerian orbits, although it gives a residual noise of 12.4 and 9.4 m s^{-1} for the two data sets.

The amplitude of this jitter is compatible with the expected jitter of 12 m s^{-1} (see Section 3). It is therefore probably caused by activity, since the average $\log R'_{\text{HK}}$ is -4.65 dex, indicative of an active star. During the period of observations, however, the stars showed almost no variation of its bisector span (r.m.s. = 15 m s^{-1}) and chromospheric activity (Fig. 1). The $\log R'_{\text{HK}}$ parameter has an r.m.s. of 0.08 dex, and its variation is not correlated with the radial velocity signal. The radial-velocity variations are only weakly correlated with the bisector span for the two signals at 12.6 and 248 days (Fig. 6). The estimated rotation period of ≈ 10 days (see Section 3) and the marginally correlated behaviour of the bisector span without the outer planet signal (Fig. 6 middle), however, might cast some doubt on the inner planet. With an amplitude of 91 m s^{-1} , it is nevertheless unlikely that the signal is entirely generated by spot activity. With an activity-induced scatter amplitude of the order of 12 m s^{-1} , spot-related activity could explain the residual noise level, but not the 12 -day period or the 91 m s^{-1} amplitude signal. Dedicated activity simulations are needed to estimate the required correction, as in Boisse et al. (2012). In Figure 7, we compare the periodogram of the radial-velocity measurements with the periodogram of the bisector spans. While the former (top plot) exhibits a strong peak at 12.6 days, the latter (bottom plot) shows faint peaks at 7.8 and

10.9 days. In this paper, we neglected the contribution of the activity to the inner-planet signal.

The best two-Keplerian model shows that the system of HD 159243 is composed of a 12.6 -day Jupiter-like planet (minimum mass of $1.13 \pm 0.05 M_{\text{Jup}}$) with a second giant planet with a minimum mass of $1.9 \pm 0.13 M_{\text{Jup}}$ in a 248 -day period. The outer planet, despite its lower amplitude, is clearly detected in the periodogram of the radial-velocity measurements without the inner-planet signal (Fig. 7, middle plot). The two planetary companions have circular orbits. Table 3 gives the parameters of the planets obtained after $500,000$ MCMC iterations. The non-detection of an astrometric signal with Hipparcos sets an upper limit of $0.52 M_{\odot}$ for the outer companion HD 159243 c, a weak constraint that can also be established independently by the non-detection of a secondary signal in the spectra.

A transit search was carried out with several telescopes despite the relatively low transit probability of 4% . Observations were carried out on 30 July 2012 at Owersky Observatory¹ (La Palma, Spain) with a 14-inch telescope. The instrument includes a CCD SBIG STL-1001e camera and a Sloan r' filter. Photometric observations were reduced using the software Muniwin 2.0. The sequence lasted 4.3 hours and the normalized flux reached a scatter of 0.7% . A second series of observations was secured on 9 April 2013 at Saint Michel l'Observatoire. It was obtained with a 20-cm telescope at $f/5.5$ equipped with an SBIG ST8XME camera during 2.2 hours; a standard deviation of the normalized flux 0.46% was measured. Two additional sequences on 4 May and 10 June 2013 made use of the ROTAT² 60-cm telescope at Haute-Provence Observatory, equipped with an SBIG STL11000 camera at the Newton focus reduced at $f/3.2$. Images of all sequences were processed with Muniwin 2.0 and relative photometry was extracted using one or several comparison stars. The first sequence of 4.1 hour duration has a scatter of 0.5% in relative flux; the second sequence lasted 3.9 hours and the flux has an r.m.s. of 0.6% . Together the photometric observations cover 75% of the transit window as allowed at the latest date of observations (June 2013). The transit ephemeris error (~ 9 hours) is now much larger than the transit duration (expected 1.8 hour). Recovering a more accurate transit ephemeris would require a new intensive radial-velocity campaign over several weeks. The standard deviation of the full photometric time series is 0.7% , and no transit is detected with a limiting depth of about 0.5% . Figure 8 shows the relative flux of HD 159243 and the expected ephemeris, duration, and depth of a potential transit, with a tolerance of 9 hours corresponding to the propagated error in mid-2013. More data are needed to conclude.

4.3. HIP 91258

The star HIP 91258 was observed with SOPHIE+ only after its major upgrade in June 2011. Twenty-seven measurements were secured on this target. The average uncertainty of this data set is 3.4 m s^{-1} . The periodogram of the RV series shows a peak at 5 days and its harmonics and aliases, as seen in Fig. 10. When modelled with a single Keplerian, we derive a standard deviation of the residuals of 45 m s^{-1} , indicating that another signal is present. The residuals drop to 13 m s^{-1} when a linear trend is added, then to 6 m s^{-1} when the trend is quadratic. Adding a second planet to the fit does not improve the residuals. The simplest and best fit is thus obtained with a quadratic trend and a short-period planet. The star does not show strong signs of

¹ <http://www.over-sky.fr/>

² <http://stargate-ohp.de/>

Table 3. Orbital and physical parameters for the planets orbiting HD 159243.

Parameter		HD 159243 b	HD 159243 c
P	[days]	12.620±0.004	248.4 ±4.9
T	[JD-2400000]	56426.11±0.21	56484±11
$T_{transit}$	[JD-2400000]	56416.78±0.22	56428±102
e		0.02±0.018	0.075±0.05
ω	[deg]	223±93	69±97
K	[m s ⁻¹]	91.1±2.1	56.6 ±3.3
$m_2 \sin i$	[M _{Jup}]	1.13±0.05	1.9±0.13
a	[AU]	0.11±0.002	0.80±0.02
γ_{SOPHIE}	[km s ⁻¹]	-22.653 ±0.012	
$\gamma_{SOPHIE+}$	[km s ⁻¹]	-22.69±0.01	
N_{meas}		53	
Span	[days]	767	
σ (O-C)	[m s ⁻¹]	12.4/9.4	
χ^2_{red}		4.2	

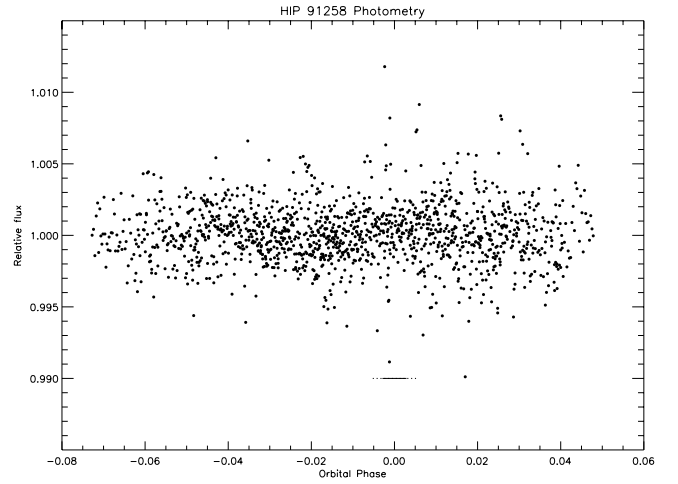
Table 4. Orbital and physical parameters for the planet orbiting HIP 91258.

Parameter		HIP 91258 b
P	[days]	5.0505±0.0015
T	[JD-2400000]	56164.275±0.028
$T_{transit}$	[JD-2400000]	56165.565±0.023
e		0.024±0.014
ω	[deg]	276±64
K	[m s ⁻¹]	130.9±1.7
$m_2 \sin i$	[M _{Jup}]	1.068±0.038
a	[AU]	0.057±0.0009
γ_1	[km s ⁻¹]	-9.452±0.002
linear	[m/s/yr]	-431±13
quadratic	[m/s/yr ²]	-1032±109
N_{meas}		27
Span	[days]	145.8
σ (O-C)	[m s ⁻¹]	5.97
χ^2_{red}		3.1

activity, with a flat bisector span as a function of the radial velocity (Fig. 11) and an r.m.s. of 8 m s⁻¹. The periodogram of the bisector spans shows only noise (Fig. 10 bottom). The log R'_{HK} value varies very little and shows no cyclic behaviour (Fig. 1), with a standard deviation of 0.03 dex during the period of observations. When the Keplerian+quadratic trend model is removed from the data, the periodogram shows a peak near 29 days that could be caused by activity, since the estimated stellar rotation period from the average log R'_{HK} index is 24±7 days.

The main detected signal is attributed to a planet with a minimum mass of 1.09 M_{Jup} in a 5.05 day circular orbit with a semi-amplitude of 130.9±1.7 m s⁻¹. The full set of parameters is given in Table 4. When a model with two Keplerian orbits is adjusted to the data, the best solution favours an outer body with a 5-yr period and a mass slightly above the hydrogen-burning limit. The time span of observations is, however, insufficient to precisely characterize of this distant body in the system of HIP 91258, and we defer its identification to future studies based on several-years long additional observations. If adjusted to the shortest possible period of 150 days and using a null eccentricity and an RV amplitude of 100 m s⁻¹ as observed, the lowest possible mass of the outer companion is 2.5 M_{Jup}. A regular RV monitoring with five to ten measurements per year over two years would provide a sufficient constraint to determine whether the outer companion is in the planet, brown dwarf or star domain. Adaptive-optics imaging or future space astrometry with GAIA of this target would also allow constraining a possible stellar companion.

The HIP 91258 b planet has a transit probability of 12%. Nine series of observations were carried out on 15 and 30 August 2012 and in May to July 2013 with the Oversky, ROTAT, BROA and Crow facilities. BROA uses a 20cm Celestron C8 with a KAF402XME camera and an R_c filter. The Crow observatory uses a 30cm aperture Meade LX200, an I_c filter, and an SBIG ST8XME camera. Combining the 47 hours of observations of this target (online Table 8), we can exclude that a transit occurred between -9 and +6 hours around the expected times for the transit center. Figure 12 shows the merged photometric light curve obtained at the expected time of transit. The r.m.s. of the measurements is 2 mmag. A transit with 0.4% depth would have been detected, while a depth of ~ 1% is expected for a Jupiter-sized planet passing across a solar-like disk.


Fig. 12. Relative flux of HIP 91258 phased with the orbital period and time of transit of companion b. The dotted line shows the 1- σ uncertainty in the transit ephemeris. The thick line shows the expected transit duration and depth for the nominal ephemeris. Transits are ruled out to a depth of ~0.4%.

5. Discussion

The stars HD 13908, HD 159243, and HIP 91258 host multiple-planet systems with at least two companions. The inner companion is a hot/warm-Jupiter-like planet and the outer companion is more massive. Each planet in the three systems thus represents one of the two main populations of giant planets: hot/warm Jupiters, and distant giant planets. Planets HD 13908 c and HD 159243 c are located inside the ice line of their respective host star. For the system around HIP 91258, the outer companion is not yet characterized, since only part of the orbit is observed, although we were able to estimate that its mass is larger than 2.5 M_{Jup}. Because the ratio of periods (inner/outer) is lower than 0.2, the three systems can be considered as stable hierarchical systems. Their dynamical evolution is not subject to mean-

motion resonance interactions but rather to secular perturbations (Beaugé et al. 2012).

Their configurations are not common, since most multiple systems are composed of low-mass planets. Other hot/warm Jupiter planets (mass greater than $0.5 M_{\text{Jup}}$ and period shorter than 20 days) with (at least) one known outer companion are: 55 Cnc b, HAT-P-13 b, HAT-P-17 b, HD187123 b, HD 217107 b, HD 38529 b, HIP 14810 b, and ν And b. All of these systems except HIP 14810 have outer planets more massive than the inner one, like the systems around HD 13908, HD 159243 and HIP 91258 (the mass of HIP 91258 c is still undetermined, but it is larger than the mass of HIP 91258 b).

Including all detection technics, there are currently 146 known multiple-planet systems³, of which 92 have (minimum) mass measurements of all companions through radial-velocity measurements. Ten of these systems have an inner planet of the hot/warm-Jupiter category (with a period shorter than 20 days), which represents 11% of them. This is compatible with the analysis of Steffen et al. (2012) from the Kepler-object-of-interest sample (Batalha et al. 2013), who have shown that planets with periods larger than 6.3 days or with a radius smaller than $0.6 R_{\text{Jup}}$ have a $\geq 10\%$ probability to have another transiting or TTV-planet in the system.

We cannot, however, derive reliable occurrence rates of hot/warm Jupiters in systems with respect to single hot-Jupiters from current observations, because the sample of multiple systems is heterogeneous and detection limits vary from one system to the other. In addition, the detection bias of radial-velocity and transit techniques favours the detection of short-period Jupiters, but severely limits the detection of outer planets: the latter requires both long-term observations and an accuracy of a few m s^{-1} for the decreasing amplitude; in addition, the transit probability decreases with increasing semi-major axis.

Multiple systems composed of giant planets can serve as important constraints for migration models. The formation of hot Jupiters is not thought to occur *in situ*, but at large distances from their central star, followed by orbital evolution due to several types of interactions in the system: interaction with the protoplanetary disks (type II migration), dynamical interactions with other planets in the system, or Kozai migration. In early papers after the discovery of 51 Peg b, the formation of a hot-Jupiter planet was shown to result from planet-planet scattering followed by tidal circularization of the inner planet (Rasio & Ford 1996), for certain initial conditions. The formation of giant planets with a massive inclined body at large distances can also result in a decrease of the physical separation between the planet and its host star, until the orbit is circularized by tides (Kozai 1962; Wu et al. 2007). The detection and characterization of systems with a hot/warm Jupiter and another outer body in the system therefore gives practical examples of the potential outcome of these mechanisms. To determine whether type II migration is the most common phenomenon for the formation of hot Jupiters, as was recently discussed by Rice et al. (2012), it would be necessary to have precise observational constraints on all single hot-Jupiter systems, to determine what types of massive outer bodies are allowed by the data. A full picture of planetary system architecture is required to understand the origins of the inner-planet migration. Interestingly, the inner planets HD 13908 b, HD 159243 b, and HIP 91258 b found in the present work do not have periods corresponding to the pile-up of hot Jupiters at a period of about three days (Udry et al. 2003, e.g.), but longer periods of 5 to 20 days. This may be a sign that their current

distance to their star originates in an evolution induced by other mechanisms than friction with the protoplanetary disks, such as planet-planet interactions (for HD 13908 b and HD 159243 b) or planet-star interactions (for HIP 91258 b, whose system may have a planetary or stellar outer companion).

The occurrence of massive planets at about 2 AU, such as HD 13908 c (mass greater than $5 M_{\text{Jup}}$) may also be an interesting constraint for the accretion model with migration, because it was shown by Alexander & Pascucci (2012) that the efficiency of accretion across the gap has a strong influence on the existence of such planets. Moreover, the planet HD 159243 c with about $2 M_{\text{Jup}}$ at 0.8 AU may correspond to the predicted pile-up of planets caused by photoevaporative clearing of the disk, as predicted in Alexander & Pascucci (2012) and observationally shown by Wright et al. (2009).

The relatively large semi-major axis of HD 13908 b and HD 159243 b fits the planet-planet scattering models with two initial planets better than those with three or four planets, if the orbital evolution of these systems is due to dynamical interactions between the planets and in the context of the simulations performed and discussed by Beaugé & Nesvorný (2012).

Our study confirmed the interest in extending the observational constraints of the exoplanet sample, in particular by following-up stars with known planets over a time scale of several years, at a precision of a few m s^{-1} . This allows one, in the long term, to assemble a more general picture of the mass distribution in the system after its dynamical evolution.

Acknowledgements. We gratefully acknowledge the Programme National de Planétologie (telescope time attribution and financial support), the Swiss National Foundation, and the Agence Nationale de la Recherche (grant ANR-08-JCJC-0102-01) for their support. R.F.D. is supported by CNES. We warmly thank the OHP staff for their great care in optimising the observations. N.C.S., I.B. and A.S. acknowledge the support of the European Research Council/European Community under the FP7 through Starting Grant agreement number 239953. N.C.S., I.B. and A.S. also acknowledge the support from Fundacao para a Ciência e a Tecnologia (FCT) through program Ciência2007 funded by FCT/MCTES (Portugal) and POPH/FSE (EC), and in the form of grants reference PTDC/CTE-AST/66643/2006, PTDC/CTE-AST/098528/2008, and SFRH/BPD/81084/2011.

References

- Alexander, R. D. & Pascucci, I. 2012, MNRAS, 422, L82
 Baranne, A., Queloz, D., Mayor, M., et al. 1996, A&AS, 119, 373
 Batalha, N. M., Rowe, J. F., Bryson, S. T., et al. 2013, ApJS, 204, 24
 Beaugé, C., Ferraz-Mello, S., & Michtchenko, T. A. 2012, Research in Astronomy and Astrophysics, 12, 1044
 Beaugé, C. & Nesvorný, D. 2012, ApJ, 751, 119
 Boisse, I., Bonfils, X., & Santos, N. C. 2012, A&A, 545, A109
 Boisse, I., Eggenberger, A., Santos, N. C., et al. 2010, A&A, 523, A88
 Bouchy, F., Díaz, R. F., Hébrard, G., et al. 2013, A&A, 549, A49
 Bouchy, F., Hébrard, G., Udry, S., et al. 2009, A&A, 505, 853
 da Silva, L., Girardi, L., Pasquini, L., et al. 2006, A&A, 458, 609
 da Silva, R., Udry, S., Bouchy, F., et al. 2007, A&A, 473, 323
 Díaz, R. F., Santerne, A., Sahlmann, J., et al. 2012, A&A, 538, A113
 Dumusque, X., Lovis, C., Ségransan, D., et al. 2011, A&A, 535, A55
 Flower, P. J. 1996, ApJ, 469, 355
 Fressin, F., Torres, G., Charbonneau, D., et al. 2013, ApJ, 766, 81
 Hébrard, G., Bonfils, X., Ségransan, D., et al. 2010, A&A, 513, A69
 Howard, A. W., Marcy, G. W., Bryson, S. T., et al. 2012, ApJS, 201, 15
 Howard, A. W., Marcy, G. W., Johnson, J. A., et al. 2010, Science, 330, 653
 Kozai, Y. 1962, AJ, 67, 591
 Mayor, M., Marmier, M., Lovis, C., et al. 2011, ArXiv e-prints
 Mayor, M. & Queloz, D. 1995, Nature, 378, 355
 Noyes, R. W., Weiss, N. O., & Vaughan, A. H. 1984, ApJ, 287, 769
 Pepe, F., Mayor, M., Galland, F., et al. 2002, A&A, 388, 632
 Perruchot, S., Bouchy, F., Chazelas, B., et al. 2011, in Society of Photo-Optical Instrumentation Engineers (SPIE) Conference Series, Vol. 8151, Society of Photo-Optical Instrumentation Engineers (SPIE) Conference Series
 Queloz, D., Henry, G. W., Sivan, J. P., et al. 2001, A&A, 379, 279

³ exoplanet.eu

- Rasio, F. A. & Ford, E. B. 1996, *Science*, 274, 954
Rice, W. K. M., Veljanoski, J., & Collier Cameron, A. 2012, *MNRAS*, 425, 2567
Sahlmann, J., Ségransan, D., Queloz, D., et al. 2011, *A&A*, 525, A95
Santos, N. C., Israelian, G., & Mayor, M. 2004, *A&A*, 415, 1153
Santos, N. C., Mayor, M., Naef, D., et al. 2000, *A&A*, 361, 265
Santos, N. C., Udry, S., Bouchy, F., et al. 2008, *A&A*, 487, 369
Sousa, S. G., Santos, N. C., Mayor, M., et al. 2008, *A&A*, 487, 373
Steffen, J. H., Ragozzine, D., Fabrycky, D. C., et al. 2012, *Proceedings of the National Academy of Science*, 109, 7982
Udry, S., Mayor, M., & Santos, N. C. 2003, *A&A*, 407, 369
van Leeuwen, F. 2007, *A&A*, 474, 653
Wright, J. T., Marcy, G. W., Howard, A. W., et al. 2012, *ApJ*, 753, 160
Wright, J. T., Upadhyay, S., Marcy, G. W., et al. 2009, *ApJ*, 693, 1084
Wu, Y., Murray, N. W., & Ramsahai, J. M. 2007, *ApJ*, 670, 820

Table 5. Radial-velocity measurements obtained with SOPHIE of HD 13908.

JD-2,400,000.	Radial Vel. [km s ⁻¹]	Uncertainty [km s ⁻¹]	Bis Span [km s ⁻¹]
54767.50725	15.7709	0.004096	0.0485
54809.37187	15.7398	0.003576	0.0588
55434.64430	15.8987	0.005186	0.0507
55434.64678	15.8843	0.002708	0.0473
55557.31431	15.9048	0.005970	0.0632
55577.30254	15.8711	0.002559	0.0435
55578.27211	15.8606	0.002622	0.0432
55579.33908	15.8671	0.003680	0.0587
55580.27264	15.8286	0.003047	0.0383
55583.33764	15.7993	0.005814	0.0338
55587.30206	15.7681	0.005788	0.0577
55587.30370	15.7798	0.005781	0.0810
55597.30251	15.8581	0.005345	0.0425
55597.30473	15.8604	0.003056	0.0478
55599.30208	15.8431	0.003126	0.0552
55620.32595	15.8071	0.005640	0.0368
55627.28875	15.7511	0.003263	0.0445
55630.27425	15.8136	0.004070	0.0385
55631.29515	15.8149	0.003895	0.0362
55638.31487	15.8406	0.006438	0.0390
55640.28324	15.7973	0.005869	0.0500
55646.28013	15.7445	0.003989	0.0450
55646.28340	15.7362	0.004105	0.0452
55646.28587	15.7423	0.004060	0.0588
55647.28173	15.7548	0.006255	0.0732
55647.28423	15.7494	0.005590	0.0468
55649.28213	15.8007	0.004157	0.0610
55649.28510	15.7988	0.004132	0.0467
55651.27797	15.8268	0.007974	0.0642
55651.28227	15.8169	0.005876	0.0510
55659.28847	15.7956	0.005162	0.0580
55663.29311	15.7276	0.005844	0.0500
55665.31366	15.7451	0.009224	0.0592
55668.30748	15.7981	0.007173	0.0258
55671.32016	15.8286	0.076182	0.5858
55672.30442	15.8348	0.008317	0.0490
55672.30767	15.8298	0.007144	0.0210
55673.31200	15.8304	0.009507	0.0373
55679.32709	15.7631	0.007806	0.0433
55683.32105	15.7058	0.010255	0.0627
55686.31406	15.7582	0.007617	0.0703
55785.59289	15.8281	0.005904	0.0387
55788.63021	15.8639	0.003961	0.0388
55795.61180	15.7901	0.005788	0.0538
55798.65008	15.7590	0.005889	0.0440
55799.64490	15.7546	0.005931	0.0663
55805.65203	15.8464	0.005956	0.0498
55813.57298	15.8410	0.005816	0.0472
55814.61203	15.8185	0.005845	0.0395
55814.61446	15.8190	0.003929	0.0650
55818.47529	15.7808	0.005786	0.0792
55827.53043	15.8895	0.005861	0.0372
55835.55372	15.7972	0.003846	0.0517
55842.55815	15.8331	0.005923	0.0245
55852.50272	15.8490	0.004825	0.0767
55856.63494	15.8036	0.004397	0.0355
55866.44310	15.9136	0.005931	0.0727
55878.38808	15.8155	0.004775	0.0468
55882.45955	15.8818	0.005872	0.0452
55904.31050	15.9184	0.004198	0.0423
55916.39987	15.8392	0.005975	0.0713
55926.29334	15.9501	0.006051	0.0603
55938.31974	15.8883	0.005845	0.0498
55957.26549	15.8872	0.005816	0.0403
55964.33337	15.9702	0.006063	0.0313
55976.25564	15.8803	0.006028	0.0392
55997.29594	15.9218	0.006099	0.0733
56017.28944	15.9437	0.003866	0.0388
56149.62463	15.9181	0.003168	0.0435
56157.62640	16.0270	0.003022	0.0420
56179.50970	16.0134	0.006138	0.0522
56188.58121	15.9200	0.003302	0.0452
56217.39032	16.0106	0.005880	0.0365
56234.46018	16.0210	0.003412	0.0427
56263.43382	15.9038	0.005837	0.0502

Table 6. Radial-velocity measurements obtained with SOPHIE of HD 159243.

JD-2,400,000.	Radial Vel. [km s ⁻¹]	Uncertainty [km s ⁻¹]	Bis Span [km s ⁻¹]
55638.66550	-22.7778	0.005466	-0.0147
55640.64998	-22.7183	0.005188	0.0188
55641.65382	-22.6864	0.004397	-0.0042
55660.64431	-22.7676	0.004966	0.0253
55662.66170	-22.7938	0.005066	0.0003
55667.63040	-22.6122	0.044468	-0.0573
55668.57948	-22.6022	0.007755	0.0077
55669.53776	-22.6204	0.005075	0.0213
55670.56762	-22.6461	0.004887	-0.0002
55671.63092	-22.6844	0.005146	0.0037
55672.59817	-22.7358	0.004716	-0.0030
55673.60054	-22.7637	0.005246	-0.0122
55675.59222	-22.7896	0.005016	-0.0085
55676.63612	-22.7635	0.005298	-0.0095
55677.57695	-22.7244	0.004942	0.0228
55679.53866	-22.6354	0.005153	0.0048
55681.50791	-22.5982	0.005064	0.0115
55682.62087	-22.5897	0.005188	0.0063
55683.51246	-22.6375	0.004798	0.0013
55697.55415	-22.6494	0.008064	0.0235
55702.44127	-22.7242	0.004866	-0.0073
55706.45624	-22.5506	0.005189	-0.0127
55745.38996	-22.5234	0.005939	-0.0060
55762.35288	-22.6625	0.005067	0.0400
55786.40889	-22.6685	0.005246	0.0257
55793.32333	-22.5896	0.005282	0.0117
55799.34877	-22.7004	0.005336	0.0030
55807.29972	-22.5930	0.005261	0.0042
55809.35545	-22.6076	0.005271	0.0168
55812.29685	-22.7347	0.005210	-0.0263
55817.28854	-22.6841	0.005230	0.0162
55818.29233	-22.6433	0.005236	0.0352
55821.28792	-22.6100	0.005261	-0.0282
55823.29087	-22.6724	0.005409	0.0058
55824.29376	-22.7166	0.005351	0.0087
55825.28511	-22.7640	0.005414	0.0105
55827.28447	-22.7866	0.005347	-0.0113
55840.28498	-22.7908	0.005293	0.0168
55841.26794	-22.7599	0.005914	0.0302
55850.25186	-22.7810	0.005410	0.0115
55878.23149	-22.7905	0.006266	-0.0050
56016.65959	-22.7076	0.005434	0.0095
56054.51930	-22.7463	0.005390	0.0013
56072.54677	-22.5910	0.004999	-0.0040
56087.53884	-22.6613	0.005896	-0.0017
56107.44685	-22.6971	0.004085	0.0097
56140.35575	-22.7320	0.004172	0.0212
56150.32715	-22.6099	0.005339	0.0163
56164.34751	-22.6744	0.005443	-0.0110
56179.35399	-22.7217	0.005514	-0.0055
56217.25185	-22.6838	0.005286	0.0157

Table 7. Radial-velocity measurements obtained with SOPHIE of HIP 91258.

JD-2,400,000.	Radial Vel. [km s ⁻¹]	Uncertainty [km s ⁻¹]	Bis Span [km s ⁻¹]
56098.51190	-9.2761	0.003419	-0.0425
56106.44881	-9.5369	0.003159	-0.0258
56113.44030	-9.2840	0.003516	-0.0310
56116.38176	-9.5416	0.003244	-0.0347
56117.39637	-9.4548	0.003378	-0.0313
56121.47155	-9.5586	0.003389	-0.0390
56122.42013	-9.4619	0.003392	-0.0237
56124.35294	-9.3156	0.003435	-0.0357
56137.46212	-9.4781	0.003403	-0.0310
56138.40492	-9.3365	0.003384	-0.0297
56140.41455	-9.4384	0.003634	-0.0072
56141.41877	-9.5549	0.003171	-0.0285
56150.33240	-9.4283	0.003407	-0.0338
56151.32785	-9.5635	0.003699	-0.0308
56152.34043	-9.5338	0.003484	-0.0298
56155.38439	-9.4415	0.003382	-0.0367
56162.31653	-9.5582	0.003383	-0.0282
56164.42055	-9.3237	0.003534	-0.0285
56172.34330	-9.5742	0.003447	-0.0300
56179.36152	-9.3549	0.003465	-0.0273
56191.32642	-9.5652	0.003415	-0.0145
56219.26892	-9.4456	0.003458	-0.0142
56225.25973	-9.4413	0.003421	-0.0420
56230.30687	-9.4572	0.003364	-0.0302
56231.23900	-9.5736	0.003082	-0.0280
56237.24078	-9.7096	0.003514	-0.0453
56244.29209	-9.5361	0.003422	-0.0347